Ground-Based Demonstration of Multiple-Input Multiple-Output Synthetic Aperture Radar Tomography

Olena Sarabakha[*], Tobias Rommel[*], Gerhard Krieger[*], Michelangelo Villano[*]

[*]Microwaves and Radar Institute, German Aerospace Center (DLR)
Weßling, GERMANY
email: olena.sarabakha@dlr.de

Abstract: *Synthetic aperture radar (SAR) tomography allows the retrieval of the vertical structure of both natural and urban scenes. However, monostatic (repeat-pass) and multistatic (single-pass) tomography do not guarantee a correct reconstruction of the vertical profile when it comes to double-bounce scattering. Multiple-input multiple-output (MIMO) SAR tomography has the potential to detect and separate the contributions of single- and double-bounce scattering, allowing a more realistic reconstruction of the scene. In particular, beamforming techniques applied to data acquired by a MIMO system allow steering independently and a posteriori the transmit and receive beams in order to scan the scene even for double-bounce scattering geometries. A ground-based MIMO SAR demonstrator has been developed in order to validate the beamforming algorithm and further investigate the behavior of double-bounce scatterers in MIMO SAR tomography. This paper presents the design of the experiment and some preliminary processing results.*

1. Introduction

Synthetic aperture radar (SAR) has been widely used in the past decades in remote sensing imaging to create two-dimensional images of a scene of interest [1]. Nevertheless, conventional SAR images are limited by the fact that all the radar echoes returning from a toroid centered at the platform position are focused in the same range-azimuth pixel, losing all information about the vertical structure of the scene. This limitation can be overcome using multiple SAR acquisitions from different cross-range (or elevation) positions, thus forming a SAR tomogram that includes information about the vertical distribution of the scatterers [2]-[4]. However, SAR tomography comes with some challenges. First, the spaceborne tomographic apertures required for high vertical resolution are usually very large, in the order of kilometers, yielding the necessity to perform all the analyses and processing in the near-field assumption, as we outlined in [5]. Second, double-bounce scattering can hinder the correct reconstruction of the vertical profile, due to incorrect positioning of the targets, which determine the double-bounce scattering, and masking of weaker scatterers due to its high backscattered power. As has already been assessed in [6], double-bounce scattering has different behaviors based on the configuration of the tomographic acquisition. A tomogram can be formed using SAR images acquired in three configurations: monostatic (repeat-pass), namely with one satellite flying several times over the region of interest and acquiring a time-series of images (or different satellites acquiring anyway independent images at different times); multistatic (single-pass), with several satellites flying in formation, where only one of them transmits and all receive, acquiring one monostatic and several bistatic images in the same pass; multiple-input multiple-output (MIMO) single-pass, always with several satellites flying in formation, but where more than one satellite transmit and ideally all receive, acquiring several monostatic and several bistatic images of the scene. This latter configuration enables the implementation of MIMO SAR tomography, which allows for the separation of multiple scattering mechanisms (e.g., single-bounce and double-bounce) in the same resolution cell [7]-[9]. A few solutions for

double-bounce scattering detection and suppression using MIMO systems have already been proposed in [10], using digital beamforming on both receive and transmit, and in [11], exploiting a variation of the compressive sensing algorithm in order to separate single- and double-bounce scattering.

2. Limitations of Monostatic and Multistatic Acquisitions

A simulation has been carried out in order to analyze the different behavior of double-bounce scattering for different tomographic acquisition modes. The simulated scene consists of a building surrounded by ground as shown in Fig. 1 (left), and the double-bounce scattering is assumed to happen between the ground and the facade of the building. Two acquisition strategies have been taken into consideration: in the first, the tomographic acquisition is monostatic (repeat-pass); in the second, a constellation of satellites flying in formation acquire a multistatic tomogram in just one pass. By comparing the resulting ground range-height images in Fig. 1 (center and right), where the contributions of single- and double-bounce have been color-coded in the radar images, it is clear that the double-bounce scattering has different effects in the two considered cases. In the monostatic repeat-pass simulation, the double-bounce response is concentrated in the equivalent corner of the ground-building structure, due to the well-known equivalence of the single- and double-bounce paths of the signal for monostatic systems. On the other hand, in the multistatic single-pass simulation, the double-bounce scattering is focused at the same slant range as the equivalent corner, but at the actual elevation position of the last scatterer that has reflected the signal. This effect is due to a residual linear phase over the tomographic aperture that depends on the baseline between satellites and also on the elevation-range ratio of the scatterer. Nevertheless, none of the images represents correctly the actual scene: in the monostatic case, the double-bounce scattering is undistinguishable from the single-bounce, and may cover neighboring scatterers with its high backscattered power; in the multistatic case, the double-bounce has a different behavior with respect to single-bounce, but may lead to artifacts (response below ground level, for example) or get mixed with neighboring scatterers. These limitations in SAR tomography can be overcome by applying a beamforming on transmit and receive algorithm to data acquired by a MIMO system.

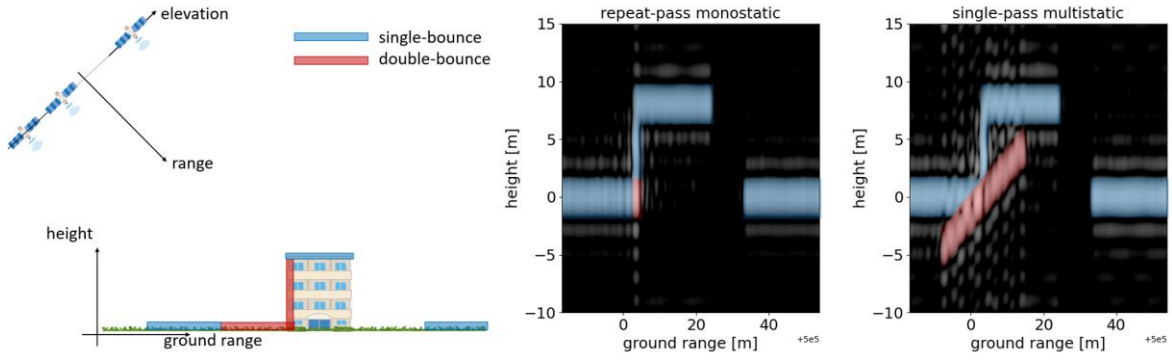

Figure 1. Sketch of the simulation geometry (left): double-bounce scattering is assumed to be occurring between the ground and the building facade (red), while the other parts of the scene (blue) respond with just single-bounce scattering. Corresponding ground range-elevation images considering a monostatic repeat-pass (center) and a multistatic single-pass (right) acquisition, where the contributions of single- and double-bounce have been color-coded, showing the different behavior of double-bounce scattering in the two cases.

Nevertheless, it has to be considered that a spaceborne MIMO SAR system would be very expensive and technically challenging. A possible way to mitigate this issue, is to reduce the

number of transmitting satellites, at the cost of introducing grating lobes (or ambiguities) in the signal. This issue can be overcome with a proper null-steering on receive in the direction where the transmit grating lobes are expected to appear.

3. Ground-Based Multiple-Input Multiple-Output SAR Demonstrator

In order to validate and further explore the possibilities offered by the proposed beamforming technique, a ground-based MIMO demonstrator has been developed. The system is based on a Vector Network Analyzer, uses a frequency-modulated, continuous-wave with center frequency 9.6 GHz and bandwidth 900 MHz, and a total of 28 identical patch antennas (12 on transmit and 16 on receive). The transmit and receive arrays are mounted on two distinct booms with a horizontal (azimuthal) separation of 30 cm in order to limit coupling and interference and with spacing of 13.6 cm and 10 cm for the transmit and receive arrays (for a total array length of 1.5 m), respectively. In order to have a full tomographic acquisition including the azimuth direction, the system is positioned on a linear axis with a slider as shown in Fig. 2 (center), which results in a total synthetic aperture of 2 m. The acquisitions along the azimuth axis are acquired with a start-and-stop strategy, with a sampling of the synthetic aperture of 5 cm, corresponding to half the physical size of the patch antenna in the azimuth direction.
The acquisitions took place from the rooftop of a building at the DLR site of Oberpfaffenhofen, with the scene of interest being on the ground in front of the building, as shown in Fig. 2 (left). The antenna arrays and the linear axis are displayed in Fig. 2 (center). The scene consisted of seven corner reflectors for calibration and two large metal plates (2 m × 1 m), orthogonal to each other, as double-bounce targets with some absorbers covering the corner (see Fig. 2 (right)). Since the observed scene is assumed to be stationary, time multiplexing was used in order to synthetize the MIMO acquisition and avoid any further complexity of the system due to orthogonal waveforms.

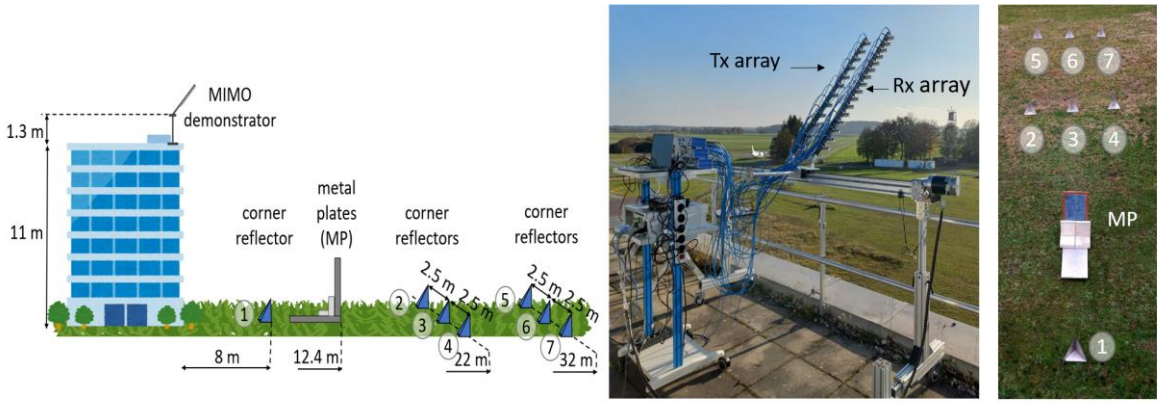

Figure 2. Sketch of the acquisition geometry (left). Antenna arrays mounted on a linear axis on the rooftop of a building during the acquisition (center). Scene of interest (right) located on the ground in front of the building. The corner reflectors are marked with the corresponding number, the metal plates are marked as "MP".

4. Preliminary Processing and Beamforming Results

As a first processing step, all images are corrected for the cable path, which is different for each antenna, and focused using a time-domain back-projection algorithm. Fig. 3 (a) shows the focused image for the couple Tx1Rx1 (topmost antennas). A similar result is obtained for all the transmit and receive couples, for a total of 192 images. The images are then co-registered using both a coarser geometric and a finer cross-correlation correction with respect to a reference image (Tx1Rx1). Fig. 3 (b) and (c) show the coherence for Tx1Rx1-Tx1Rx2 and Tx1Rx1-Tx12Rx16, respectively, which represent the shortest and longest baselines. Fig. 3 (d) shows the expected baseline and signal-to-noise ratio coherence contributions and compares the total measured coherence with the expected one for the two cases. The ground clutter is still correlated for Tx1Rx1-Tx1Rx2 in the near range and completely decorrelated for Tx1Rx1-Tx12Rx16, due to the baseline decorrelation. Note that the critical baseline varies strongly throughout the scene for Tx1Rx1-Tx12Rx16 due to the significant variation of the incidence angle. In general, the measured decorrelation is in good agreement with the expected one for both cases, as shown in Fig. 3 (d) (bottom plots). The coherence is high on the corner reflectors and on the metal plates for Tx1Rx1-Tx1Rx2, but not for the corner reflector 1 and the metal plates for Tx1Rx1-Tx12Rx16 due to the bistatic geometry (large relative angle between Tx and Rx).

Afterwards, the beamforming on transmit and receive proposed in [10] has been applied to the 192-image stack. In particular, a set of 192 weights (one for each image) can be defined to steer the transmit and receive beams in desired directions. If the same direction is selected for both the transmit and receive beams, it is possible to scan all ground ranges and display the output intensity for each ground range. This is plotted in Fig. 4 (left) for a specific azimuth

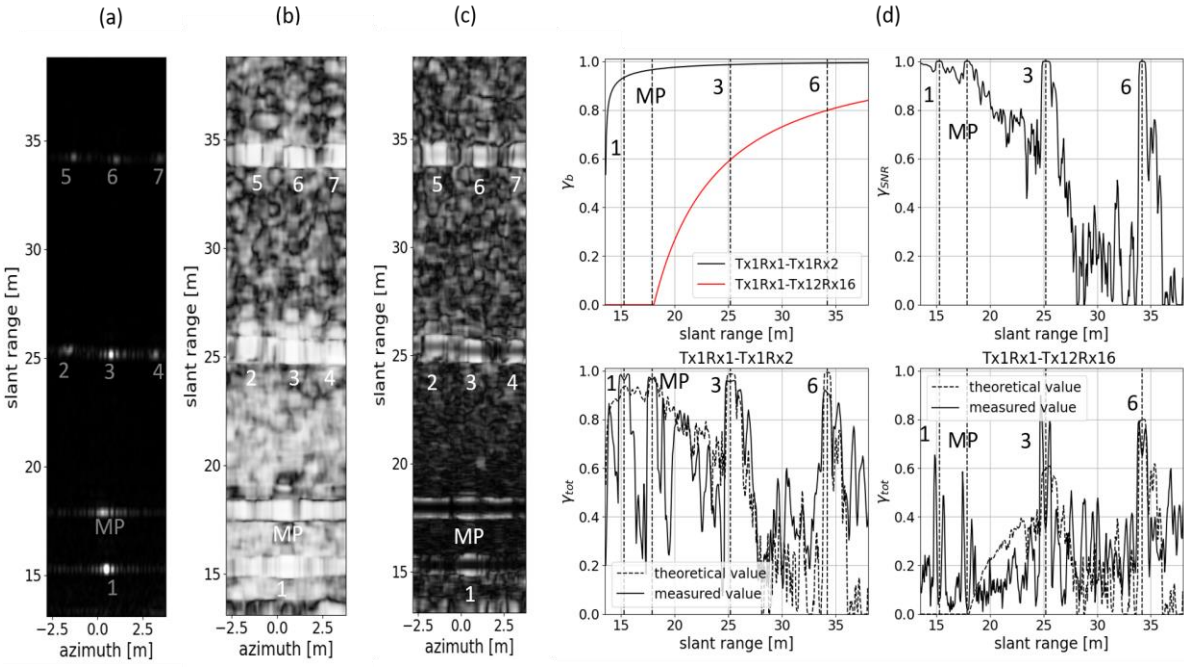

Figure 3. The focused image for the transmit-receive couple Tx1Rx1 is shown in (a); in (b) and (c), the coherence amplitude for the interferometric couples Tx1Rx1-Tx1Rx2 and Tx1Rx1-Tx12Rx16, respectively; in (d), the baseline, γ_b, and signal-to-noise ratio, γ_{SNR}, coherence contributions, and the total expected coherence, γ_{tot}, in dashed line vs. the measured coherence in solid line both for Tx1Rx1-Tx1R2 and Tx1Rx1-Tx12Rx16. The slant range positions of the targets are marked with the vertical dashed line. The corner reflectors are marked with the corresponding number, the metal plates are marked as "MP".

corresponding to the position of the metal plates. Furthermore, it is possible to point the transmit and receive beams with a fixed angle difference (or offset) $\Delta\theta$ and scan again all ground ranges and display the output intensity. This is plotted in Fig. 4 (right) for $\Delta\theta = 6.36°$ for the same azimuth position. The offset $\Delta\theta$ has been selected in such a way that the transmit beam points to the center of the vertical metal plate, while the receive beam is symmetrically pointed to the center of the horizontal metal plate. This corresponds to a $+3.18°$ steering of the Tx beam and a $-3.18°$ steering of the Rx beam with respect to elevation zero for each range position.
The single-bounce response is expected to be stronger when the two beams are pointed in the same direction, while the double-bounce response should be stronger when the beams are pointed in such a way to illuminate one surface of the double-bounce scatterer while receiving from the other, orthogonal surface, which reflects the signal to the radar system.
From the resulting profile in Fig. 4 (left), it is clearly visible that the responses of the corner reflector 1 and 3 are at least 7 dB stronger than the response from the metal plates. The response of the dihedral structure is well visible despite the absorbing material at the corner as the double-bounce response leaks into the sidelobes of the receive array. A significant attenuation can be noticed, if tapering is applied. The response of corner reflector 6 is much weaker because the selected azimuth does not exactly correspond to its position. On the other hand, when the receive and transmit beams are pointed with an offset $\Delta\theta = 6.36°$, corresponding to the centers of the two metal plates, the response of the dihedral structure is stronger than those of the corner reflectors. In particular, the response of corner reflector 3 decreases by about 20 dB, and that of corner reflector 6 by 10 dB. The response of corner reflector 1 is not significanly suppressed, as it is very close to the radar system and its reflected power still leaks into the receive beam.
These results represent some first steps in the demonstration of the capability of the developed ground-based MIMO demonstrator to acquire a MIMO stack and the possibility to discriminate *a posteriori* single- and double-bounce targets present on the scene using a beamforming on transmit and on receive algorithm.

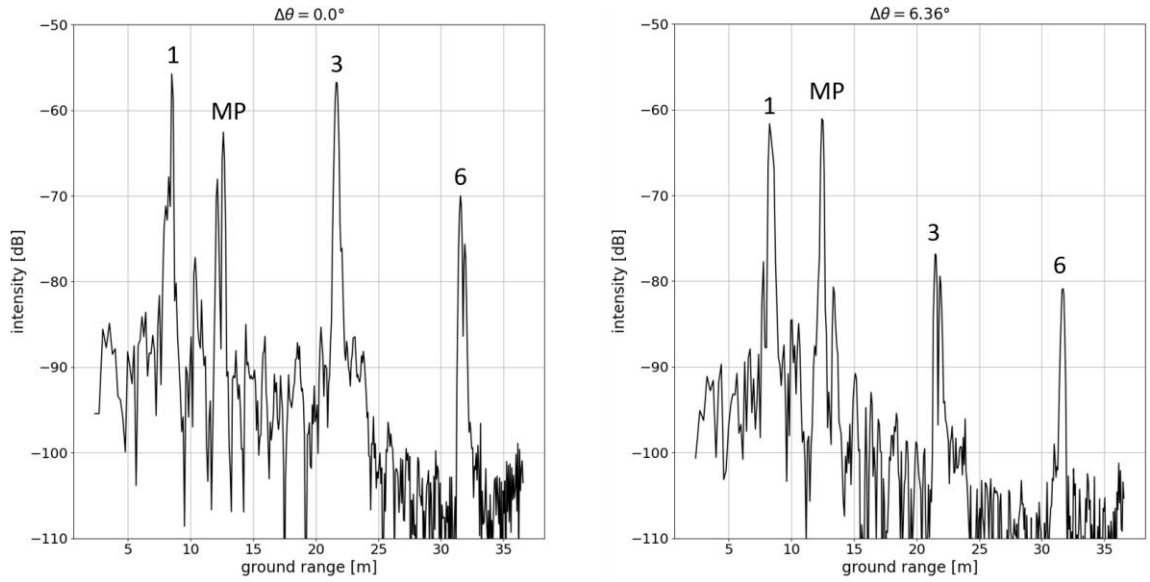

Figure 4. Ground range profiles obtained with beamforming on transmit and on receive exploiting the MIMO acquisition: transmit and receive beams steered in the same direction (left), and with an offset angle $\Delta\theta = 6.36°$ (right). These profiles are obtained processing a cut in azimuth corresponding to the position of the metal plates. The corner reflectors are marked with the corresponding number, the metal plates are marked as "MP".

5. Conclusions

A ground-based demonstrator for MIMO SAR tomography has been developed in order to perform further analyses and validate the proposed techniques with real data. An analysis on the decorrelation of the generated tomographic stack has been carried out in order to assess the quality of the coherence between the images. Beamforming both on transmit and on receive has been applied to the acquired stack in order to validate the ability of MIMO SAR tomography to discriminate between single- and double-bounce scattering. Future work includes an optimization of the beamforming algorithm and an analysis on the possibility to use less transmit elements.

Acknowledgement

This work was partially funded by the European Union (ERC, DRITUCS, 101076275). Views and opinions expressed are however those of the authors only and do not necessarily reflect those of the European Union or the European Research Council Executive Agency. Neither the European Union nor the granting authority can be held responsible for them.

References

[1] A. Moreira, P. Prats-Iraola, M. Younis, G. Krieger, I. Hajnsek and K. P. Papathanassiou, "A tutorial on synthetic aperture radar", in IEEE Geoscience and Remote Sensing Magazine, vol. 1, no. 1, pp. 6-43, March 2013.

[2] A. Reigber, A. Moreira and K. P. Papathanassiou, "First demonstration of airborne SAR tomography using multibaseline L-band data", IEEE 1999 International Geoscience and Remote Sensing Symposium. IGARSS'99 (Cat. No.99CH36293), Hamburg, Germany, 1999, pp. 44-46 vol.1.

[3] G. Fornaro, V. Pascazio, “SAR Interferometry and Tomography: Theory and Applications”, Academic Press Library in Signal Processing, Volume 2, 2014, Pages 1043-111.

[4] H. Aghababaei et al., "Forest SAR Tomography: Principles and Applications", in IEEE Geoscience and Remote Sensing Magazine, vol. 8, no. 2, pp. 30-45, June 2020.

[5] O. Sarabakha, T. Rommel, G. Krieger, M. Villano, “Separation of Scattering Mechanisms Through Multiple-Input Multiple-Output Synthetic Aperture Radar Tomography”, Kleinheubach Conference, September 2024.

[6] G. Krieger, T. Rommel and A. Moreira, “MIMO-SAR Tomography”, EUSAR, June 2016.

[7] G. Krieger, "MIMO-SAR: Opportunities and Pitfalls", in IEEE Transactions on Geoscience and Remote Sensing, vol. 52, no. 5, pp. 2628-2645, May 2014.

[8] G. Krieger et al., "MIMO-SAR and the orthogonality confusion", 2012 IEEE International Geoscience and Remote Sensing Symposium, Munich, Germany, 2012, pp. 1533-1536.

[9] G. Krieger et al., "Digital beamforming and MIMO SAR: Review and new concepts", EUSAR 2012; 9th European Conference on Synthetic Aperture Radar, Nuremberg, Germany, 2012, pp. 11-14.

[10] T. Rommel and G. Krieger, "Detection of Multipath Propagation Effects in SAR-Tomography with MIMO Modes", Proceedings of EUSAR 2016: 11th European Conference on Synthetic Aperture Radar, Hamburg, Germany, 2016, pp. 1-5.

[11] F. Zhang, X. Liang, R. Cheng, Y. Wan, L. Chen and Y. Wu, "Building Corner Reflection in MIMO SAR Tomography and Compressive Sensing-Based Corner Reflection Suppression", in IEEE Geoscience and Remote Sensing Letters, vol. 17, no. 3, pp. 446-450, March 2020.